



Available online at www.sciencedirect.com

ScienceDirect

www.elsevier.com/locate/jes

JES
JOURNAL OF
ENVIRONMENTAL
SCIENCES
www.jesc.ac.cn

A review of functions and mechanisms of clay soil conditioners and catalysts in thermal remediation compared to emerging photo-thermal catalysis

Juan Zhang^{1,***}, Shuo Wang^{1,**}, Xin Wang¹, Wentao Jiao²,
Minghua Zhang³, Fujun Ma⁴

¹ State Key Laboratory of Advanced Metallurgy, School of Metallurgical and Ecological Engineering, University of Science and Technology Beijing, Beijing 100083, China

² Research Center for Eco-Environmental Sciences, Chinese Academy of Sciences, Beijing 100085, China

³ College of Agricultural and Environmental Sciences, University of California, Davis, CA 95616, USA

⁴ State Key Laboratory of Environmental Criteria and Risk Assessment, Chinese Research Academy of Environmental Sciences, Beijing 100012, China

ARTICLE INFO

Article history:

Received 21 June 2023

Revised 9 November 2023

Accepted 10 November 2023

Available online 17 November 2023

Keywords:

Persistent organic contaminants

Clay soils

Thermal remediation

Soil conditioning

Synergistic catalysis

ABSTRACT

High temperatures and providing sufficient time for the thermal desorption of persistent organic pollutants (POPs) from contaminated clay soils can lead to intensive energy consumption. Therefore, this article provides a critical review of the potential additives which can improve soil texture and increase the volatility of POPs, and then discusses their enhanced mechanisms for contributing to a green economy. Ca-based additives have been used to reduce plasticity of bentonite clay, absorb water and replenish system heat. In contrast, non-Ca-based additives have been used to decrease the plasticity of kaolin clay. The soil structure and soil plasticity can be changed through cation exchange and flocculation processes. The transition metal oxides and alkali metal oxides can be applied to catalyze and oxidize polycyclic aromatic hydrocarbons, petroleum and emerging contaminants. In this system, reactive oxygen species ($\bullet\text{O}_2^-$ and $\bullet\text{OH}$) are generated from thermal excitation without strong chemical oxidants. Moreover, multiple active ingredients in recycled solid wastes can be controlled to reduce soil plasticity and enhance thermal catalysis. Alternatively, the alkali, nano zero-valent iron and nano-TiN can catalyze hydrodechlorination of POPs under reductive conditions. Especially, photo and photo-thermal catalysis are discussed to accelerate replacement of fossil fuels by renewable energy in thermal remediation.

© 2024 The Research Center for Eco-Environmental Sciences, Chinese Academy of Sciences. Published by Elsevier B.V.

Introduction

Soil contamination and deterioration cause emerging threats to climate sustainability, food security and human health

(Amundson et al., 2015). The soils across China were mostly contaminated by heavy metals, hexachlorocyclohexanes (HCHs), dichlorodiphenyltrichloroethanes (DDTs) and polycyclic aromatic hydrocarbons (PAHs) (MEE, 2014). The lead, petroleum, asbestos, and PAH contaminants were commonly found at brownfield sites and received cleanup grants from the United States Environmental Protection Agency (US EPA, 2019). In the surveyed European Environment Agency member countries and cooperating countries, it is urgent to control min-

* Corresponding author.

E-mail: zhangjuan85@ustb.edu.cn (J. Zhang).

** These authors contributed equally to this work.

eral oils consisting of petroleum hydrocarbons (PHs) and PAHs, heavy metals, as well as organochlorine pesticides (OCPs) including HCHs and DDTs from agricultural production (EEA, 2020; Wang et al., 2019a; Zhang et al., 2018).

The thermal treatment method is a highly efficient and safe technique for the remediation of industry-impacted soils/sediments contaminated with kinds of above-mentioned persistent organic pollutants (POPs) and some metals (Davin et al., 2021; Ossai et al., 2020). In a thermal desorption (TD) heating system at low temperatures of 90°C to 320°C (LTTD) or high temperatures of 320°C to 540°C (HTTD), the organic contaminants can be removed from soil, sludge and sediments through mechanisms of evaporation, oxidation, pyrolysis, hydrolysis, incineration, or thermal cracking (Ossai et al., 2020; Smarzewska and Guziejewski, 2021; Zhao et al., 2019a). In comparison to in situ TD for source contamination, high-cost ex situ TD is applied for excavated soil contamination by high concentrations and high risks of organic contaminants and heavy metal mercury (Falciglia et al., 2011a; Smarzewska and Guziejewski, 2021; Zhao et al., 2019a).

The use of HTTD for the removal of POPs and mercury with high boiling points from clays and organic soils would require high energy and economic costs, and lead to changes of soil composition, pH and biodiversity (Han et al., 2020; O'Brien et al., 2018; Teng et al., 2020; Vidonish et al., 2016). More abundant aromatic and aliphatic structures of soil organic matters (SOM) and inter-crystalline porous structures have been linked to silt and clay fractions of soil (fine particles) (Cheng et al., 2021; Falciglia et al., 2011a, 2016). Furthermore, the high molecular weight and high-dielectric (polar) PAHs are primarily bound to the aromatic structures of SOM, followed by clay minerals (Cheng et al., 2021; Falciglia et al., 2016). The interstratified (mixed-layer) structures and interlayer spacing of clay are formed by different ratios of illite to smectite (also called montmorillonite) minerals and exchangeable cations, which play vital roles in the entrapment of organic contaminants by soil (Dai et al., 2020; Xiao et al., 2022). In addition, the heat transport is reduced for clay soils by agglomeration (cementation) and adhesion to TD equipment (Falciglia et al., 2011a; Zhao et al., 2019a).

The common soil dryer quicklime (CaO) can reduce the soil viscosity and plastic index (PI), increase the particle size of soils and further enhance TD efficiency (Dash and Hus-sain, 2012; Vitale et al., 2020; Zhao et al., 2019a). The ability of magnesium (hydr)oxide, silica, alumina, ferrous slag and fly ash to improve soil plasticity have been explored (Goodarzi and Salimi, 2015; Jafer et al., 2018; Kalhor et al., 2019; Shalabi et al., 2017; Ureña et al., 2013). In addition to soil texture improvement, POPs can be catalyzed and degraded into low molecular weight and high vapor pressure species, which are then desorbed at lower temperatures (Liu et al., 2014, 2015a, 2015b, 2019a; 2020). There are various additives chosen for catalytic degradation of halogenated or non-halogenated POPs (Cassidy et al., 2015; Hu et al., 2019; Karaca et al., 2016; Sliem et al., 2019).

The additive was previously reviewed as an important influencing factor for TD (Wang et al., 2021; Zhao et al., 2019a). However, they did not fully review types of soil additives and their enhancement mechanisms based on soil textures and

behaviors of different POPs. Therefore, through systematically hand searching references in the academic literature databases (Appendix A Text S1), this study groups additives into Ca based, non-Ca based, and recycled solid wastes as conditioners of clay soils with different composition and plasticity. Moreover, oxidation and reduction catalysts that can improve degradation of different POPs along with their enhanced mechanisms are reviewed to explore the behaviors of POPs during remediation processes. In particular, we try to explore high efficiency and green photocatalysis synergistic thermal remediation against Fenton's reaction-based chemical oxidation and thermal catalysis in the new green economy.

1. Adsorption and thermal desorption of various organic contaminants in soils

The contaminants (fractions of PHs, PAHs, PCBs, Pentachlorophenol and HCH) with different physical and chemical properties are desorbed from two types of soil (sandy soil and clay soil) at different temperatures through different mechanisms (Appendix A Table S1 and Fig. 1). PHs from C10 to C22 are physically adsorbed on soils by Van der Waals and hydrophobic forces (Li et al., 2020). For sandy soil, most PHs (C10 to C16) are removed at 90°C to 200°C through air entrainment, contaminant evaporation and boiling, in addition, the evaporation and boiling of PHs (C16 to C22) occur when the temperatures reach 200°C to 300°C (Falciglia et al., 2011b; Li et al., 2020). The PHs (C22 to C28) are adsorbed on soils by weak hydrogen bonds and dipole bonds and they can be removed at 300°C to 400°C through evaporation and boiling (Liu et al., 2019a, 2020). The strong electrostatic and π - π stacking interactions between PHs (C28 to C40) and soil have been attributed to aromatic ring structures, hydroxyl groups and amino groups (Li et al., 2020). They can be removed at 500°C to 540°C by evaporation, boiling and cracking, and the alkenes generated from breaking of C-H and C-C bonds of saturated linear alkanes are removed by a boiling process (Li et al., 2020; Ren et al., 2020). For clay soil, higher temperatures of 150°C to 400°C are required for the removal of PHs (C10 to C22) that are hydrophobically adsorbed on soil with a higher specific surface area (Falciglia et al., 2011b; Li et al., 2016, 2020). For clay soils with high moisture content, the thermal desorption efficiencies of contaminants often decrease owing to the heat loss associated with excessive water evaporation and the trapping of contaminants in the intercrystalline water layer (Zhao et al., 2019a).

PAHs with two or more fused aromatic rings and polychlorinated biphenyls (PCBs) with chlorine substitutions at the biphenyl ring are adsorbed on soils by hydrophobic forces, O-H- π effects and π - π stacking interactions (Cheng et al., 2021; Valizadeh et al., 2021, 2022). For sandy soil, PAHs are desorbed at 100°C to 400°C through air entrainment, evaporation and boiling (Chen et al., 2020a; Jeon et al., 2013). The macromolecular aromatics and asphaltenes in petroleum colloids are recalcitrant to removal and can be carbonized into ecologically-friendly coke residue trapped in soil through dehydrogenation, condensation and oligomerization processes at 400°C to 540°C (He et al., 2020; Zhang et al., 2021a). Owing to stronger adsorption of PAHs on clay soil and the

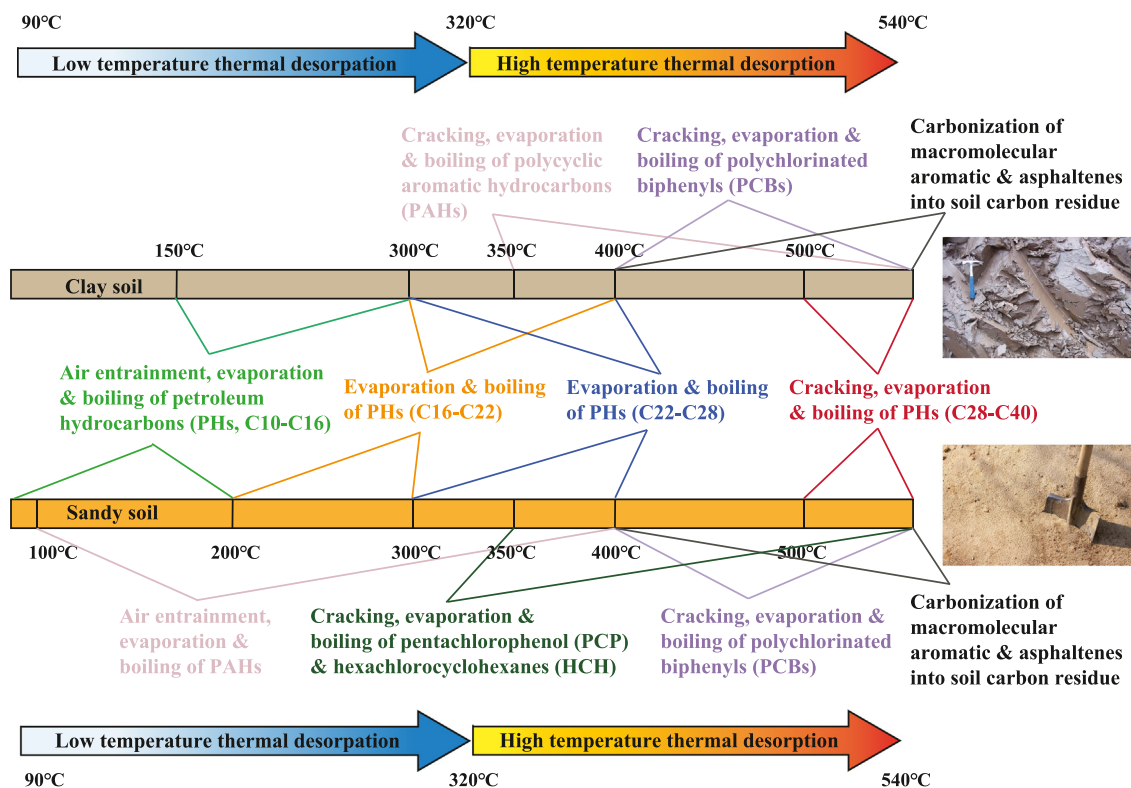


Fig. 1 – Mechanisms of thermal desorption of organic contaminants (PHs, PAHs, PCBs, PCP and HCH) from clay soil and sand soil at different temperatures.

temperature-induced polymerization between PAHs and SOM, PAHs are firstly broken up into the low molecular weight aromatic structures and alkanes at temperatures higher than 350°C, and then are removed through evaporation and boiling (Biache et al., 2015a). For high-chlorinated organic contaminants, the pentachlorophenol and hexachlorocyclohexanes with a six-carbon ring are removed from sandy soil at 350°C through evaporation, boiling and cracking, and the PCBs with biphenyl ring are removed from both sandy soil and clay soil at 400°C to 540°C (Araújo et al., 2016; Liu et al., 2014). These high-chlorinated contaminants are first dechlorinated by water and soil organic matter acting as hydrogen sources, followed by breaking of the aromatic structures, and the C-H and C-C bonds (Thuan and Chang, 2012).

2. Different types of additives acting as clay soil conditioners

2.1. Ca-based and non-Ca-based additives

(MgO/Mg(OH)₂ and SiO₂)

A certain ratio of CaO/Ca(OH)₂ to soil (1% to 10%) of strong base-lime (pH: 12 to 13) is often used to improve the plasticity, swelling, pore diameter and stability of expensive clay soil (Appendix A Table S2). The liquid limit and plastic limit of soil represent the amounts of water addition needed in order to change them from plastic to liquid states and from semisolid to plastic states, respectively (Budhu, 2010). The plasticity index (PI) is defined as the difference in values between the liq-

uid limit and the plastic limit, which can always be reducing until the soil pH approaches 12.40 by successive addition of 10% hydrated lime into bentonite clay (Al-Mukhtar et al., 2010; Elert et al., 2017). The lime can effectively reduce the PI of smectite rather than kaolinite or sulfate-rich illite clay (Cheshomi et al., 2017; Dash and Hussain, 2012; Vitale et al., 2020). These clay minerals are detailedly described in Section 2.3. Heat is also released from the hydration reaction of CaO acting as a common dryer (Zhao et al., 2019a).

Non-Ca-based additives, such as MgO/Mg(OH)₂ (5% to 15%) with alkalinity (pH 10.3) lower than Ca-based additives and nano-SiO₂ (0.5% to 4%), can also reduce the PI of soils (Appendix A Table S3). However, Mg-rich lime (MgO and CaO composites) is a better soil conditioner and its combined effect on the PI of marly clay is higher than those of single CaO or single MgO (Elert et al., 2017). Nano-SiO₂ was reported to reduce the PI of low plasticity clay (PI: 11.4–18) because of its high hydroscopicity, great specific surface area and high surface charge (Buazar, 2019; Kalhor et al., 2019).

2.2. Composite additives and re-utilization of slag, ashes and eggshell

It is essential to explore the re-utilization and directive control of industrial wastes such as ferrous slags and fly ashes containing lime and other active components, a pathway to a low carbon economy (Goodarzi and Salimi, 2015; Jafer et al., 2018). Indeed, many types of ferrous slags and fly ashes have been used as the plasticity conditioners of different soils and their effects depend on the types and amounts of additives

and auxiliary additives (Appendix A Table S4). Compared with above mentioned Ca-based and non-Ca-based additives (at dosages lower than 15% in Appendix A Tables S2 and S3), higher amounts (2%–30% in Appendix A Table S4) of ferrous slags are added to improve soils. The PI of clay soil is slightly reduced from 24 to 22 by 5% coarse steel slag (Shalabi et al., 2017), which is less effective than the steel refining slag used in our study. The lime or MgO as auxiliary additive is used for the directive control of the compositions of ash and slag through hydration of Ca_2SiO_4 and Ca_3SiO_5 to generate more dissolved Ca^{2+} and enhance their effects on clay soil (Feng and Sun, 2020; Modarres and Nosoudy, 2015; Salimi and Ghorbani, 2020). These additives as well as eggshell (CaCO_3) and plant ash (K_2CO_3) reported by Chen et al. (2020a) have the potential to alleviate formation of large lumps via sintering and agglomeration of thermally treated soils, to avoid negative effects of high temperature on soil and thus to enhance TD efficiency and competitive advantage.

2.3. Mechanisms of clay soil conditioners

The diffuse double layer (DDL in Fig. 2) is formed by the water and cations that are absorbed on the surface of negatively charged soil particles, as described in detail by Budhu (2010). The soil liquid limit and plasticity increased with the thickness of the DDL which is affected by the soil mineral composition, pH and cations (Barker et al., 2006; Tournassat et al., 2011; Vitale et al., 2020). As shown in Appendix A Fig. S1, the clay mineral layers consisting of one silica tetrahedron sheet and one alumina octahedron sheet are tightly connected by hydrogen bonds for kaolinite, while the layers consisting of one alumina sheet sandwiched by two silica sheets are connected by weak van der Waals forces for smectite and are connected by K^+ for illite (Budhu, 2010). In addition, Na montmorillonite (a typical smectite) in Fig. 2a has a layer structure of dispersive tetrahedra-octahedra-tetrahedra which results in a far larger interlayer distance, larger surface area, higher water absorption and higher cation exchange capacity (CEC) than kaolinite and illite (Tournassat et al., 2011).

The cation exchange reaction plays a more important role in reducing the plasticity of smectite, while flocculation is more important for reducing the plasticity of kaolinite (Vitale et al., 2020). The effects of soil conditioners on the liquid limit, plastic limit and PI of clay soils and their mechanisms are summarized in Fig. 2. For the cation exchange reaction in Fig. 2a, the multivalent cation Me^{2+} (Ca^{2+} and Mg^{2+}) from soil conditioners substitutes for the Na^+ on the surface of the clay soil with high plasticity, resulting in declines in the DDL thickness, liquid limit and PI (Barker et al., 2006; Chen et al., 2020b). In Fig. 2b, the concentrations of cations and the viscosity of water in the spaces between fine particles increases, and thus the interparticle shear resistance and plastic limit also increase (Dash and Hussain, 2012). In Fig. 2c, the fine particles flocculate and the coarse particles form owing to the increases in pH and MeOH^+ by adding more soil conditioners (Vitale et al., 2020). Finally, both the liquid limit and plastic limit increase, and PI is reduced simultaneously. This can be explained by the enhancements in soil pore water and the interparticle resistance against movement (Dash and Hus-

sain, 2012), and facilitates the diffusion of contaminants from clay soil to gas phase during TD treatment (Wang et al., 2021; Zhao et al., 2019a).

3. Oxidation catalysts and reduction catalysts

3.1. Iron oxides, titanium oxides and other transition metal oxides

Iron oxide has the advantages of being low cost, abundant, and environmental-friendly, and can provide reactive radicals for thermal catalysis, photocatalysis, and other catalytic reactions, to improve their efficiency (Appendix A Tables S5 and S6). The thermal removal efficiency of PHs in sandy soil was reported to increase from 70.3% to 95.8% by adding Fe_2O_3 and Fe_3O_4 containing Fe^{3+} and Fe^{2+} had more significant effect on enhanced thermal removal of pyrene than Fe_2O_3 (Liu et al., 2020, 2021; Oden et al., 2022). Instead of harmful chemical oxidants (H_2O_2 and persulfate) involved in Fenton and Fenton-like reactions (Mirzaee et al., 2017; Usman et al., 2012), PAHs can be removed by the reactive superoxide radical ($\bullet\text{O}_2^-$) and hydroxyl radical ($\bullet\text{OH}$) generated from $\text{Fe}(\text{III})/\text{Fe}(\text{II})$ cycle combined with $\text{O}_2/\text{H}_2\text{O}$ photocatalysis reactions, a green technology (Jia et al., 2012; Luo et al., 2018, 2021; Marquès et al., 2020). And under ultraviolet irradiation, iron oxide in red soil can react with oxalic acid, a natural organic acid to form $\text{CO}_2\bullet^-$, $\bullet\text{O}_2^-$ and $\bullet\text{OH}$ and spontaneously degrade PAHs (Wang et al., 2009). It is vital to explore green oxidants and additives with a wide light absorption range like FeCl_3 , FeC_2O_4 and the nano- Fe_3O_4 coating materials in photo-synergistic promoted catalytic oxidation reactions (Jia et al., 2012; Luo et al., 2018, 2021; Wang et al., 2019b).

TiO_2 is a typical thermal catalyst and photocatalyst for removing organic contaminants from soil, sediments and industrial slurry because of its lack of toxicity, relatively high activity, good physical and chemical stability and low cost (Appendix A Table S5). In our study, the TD removal efficiency of PAHs in clay soil was enhanced from 71.0% to 99.9% at a temperature of 350°C using 2% nano- TiO_2 and air as the oxidant. The thermal removal efficiency of total oil contaminants in oily sludge increased from less than 70% to 82.69% at a temperature of 230°C by adding 1.5% nano- TiO_2 (Dang et al., 2021). High molecular weight contaminants can be decomposed into low molecular weight hydrocarbons, and completely degraded into CO_2 and H_2O using TiO_2 as the thermal catalyst and air as the oxidant (Shinbara et al., 2005; Ueta et al., 2014). In photo catalysis and photo-synergistic system, TiO_2 and its composites containing more groups for adsorption of different pollutants and wide spectrum light can effectively remove PAHs, diphenylarsinic acid and organophosphorus herbicide from soil, quartz sand, industrial sludge and sediment using light energy (Appendix A Table S5). However, water was found to be essential for the UV-photocatalytic removal of PAHs and diphenylarsinic from soil to improve the light penetration and formation of $\bullet\text{OH}$ (Dong et al., 2010a, 2010b; Gu et al., 2012; Eker and Hatipoglu, 2019; Wang et al., 2016).

The oxides of other transition metals such as Mn, Co, Zr, Ni and Zn have been explored in the oxidation of PAHs or

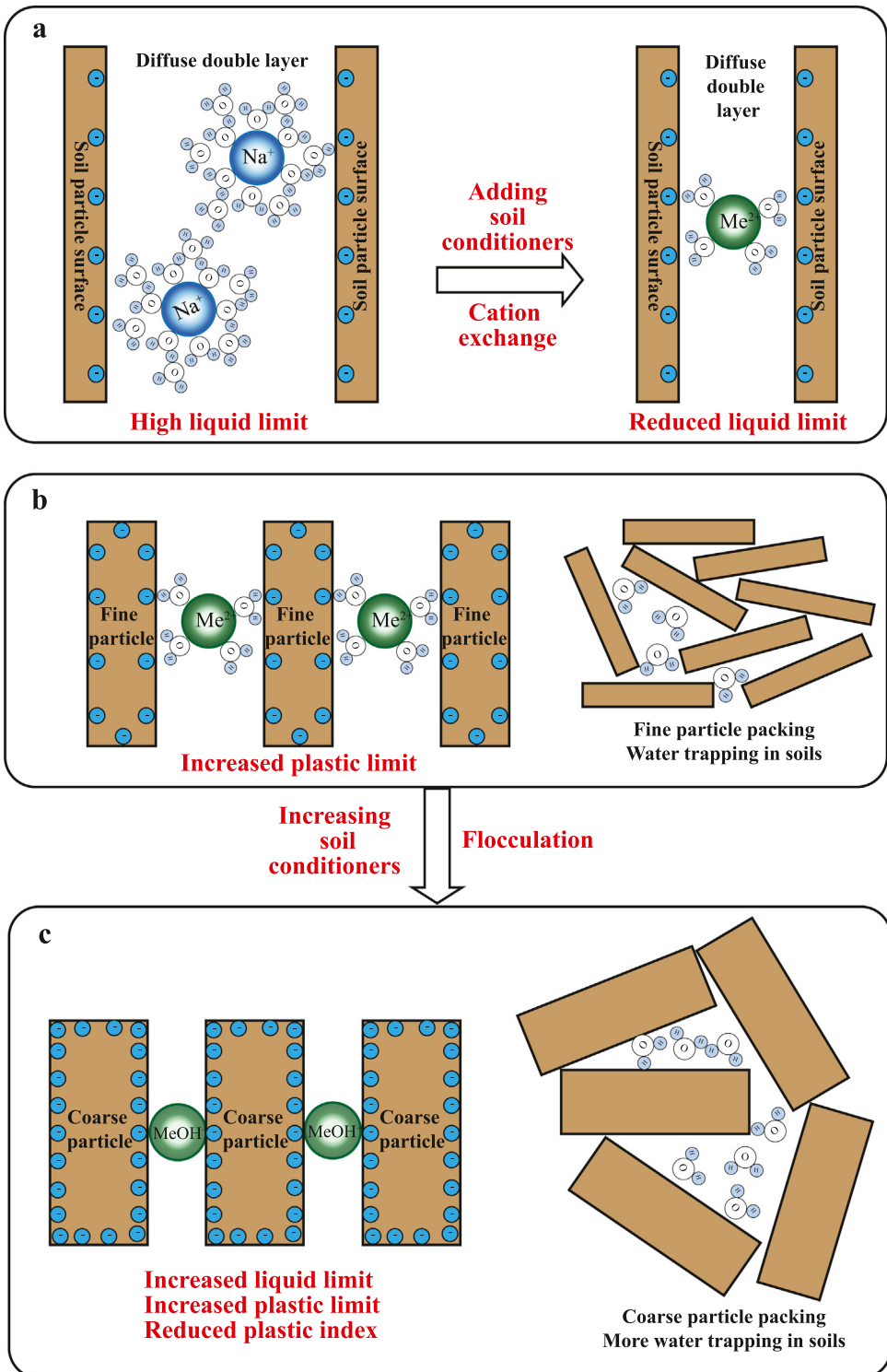


Fig. 2 – Effects and mechanisms of conditioners on the liquid limit, plastic limit and plastic index of clay soils. (a) Cation exchange reaction on the surface of clay soil with high plasticity by adding soil conditioners. (b) Interaction between fine particles with reduced diffused double layer and the liquid limit. (c) Flocculation results in an increase in particle size and a decrease in the plastic index with increasing alkalinity. Me²⁺: multivalent cations such as Ca²⁺ and Mg²⁺.

petroleum through thermal catalysis and other catalytic reactions (Appendix A Table S5). The higher removal efficiency of pyrene was obtained using thermal or photo catalytic oxidation of δ -MnO₂ than Fe or Ti oxides (Chang Chien et al., 2011a, 2011b; Oden et al., 2022). The amorphous MnO₂ and Fe(III) modified Mn oxide minerals (especially acid birnessite) possessed higher ratio of Mn³⁺ (Fe³⁺) to Mn⁴⁺ and higher concentration of oxygen vacancy, which exhibited higher thermal catalytic efficiency to oxidize anthracene and benzo(a)pyrene than other MnO₂ polymorphs (Cheng et al., 2022; Wang et al., 2020). The thermally catalytic cracking of oil sand bitumen can be improved by doping nano-sized ceria-based catalysts (CeO₂) with the transition metal oxides (ZrO₂, Fe₂O₃, or CoO) to obtain more oxygen vacancy without adding harmful ClO₂ and peroxyomonosulfate as in Fenton-like reaction (Ajumobi et al., 2018; Liu et al., 2022; Lyu et al., 2019).

3.2. Alkali/alkaline earth metal oxides and recycled solid wastes

In addition to transition metal oxides, the alkali/alkaline earth metal (hydrated)oxides and carbonates, also divided into Ca-based and non-Ca-based additives, can be used to promote the thermal cracking of PAHs and petroleum contaminants (Appendix A Table S5). The thermal catalytic removal of PHs from sandy soil can be effectively improved by CaO and non-Ca-based additives (K₂CO₃, Al₂O₃ and aluminosilicates) at the temperature of 400°C under an inert atmosphere, and K₂CO₃ worked better than other catalysts (Liu et al., 2021). The removal of saturates, aromatics, resins and asphaltenes from oily sludge were efficiently enhanced after addition of 5% KOH at the temperature of 600°C, but more KOH was ineffective (Lin et al., 2017). However, we identified that CaO promoted the aromatization of SOM and increase of PAHs in clay soil at the temperature of 400°C under an oxygen deficient atmosphere. The mixture of Ca-based and non-Ca-based additives (Ca(OH)₂ and NaHCO₃) facilitated the removal of PAHs from petroleum sludge cake under air flow (Pakpahan et al., 2013). The low cost, abundant and environmental-friendly dolomites was calcined to produce mixture of Ca-based and non-Ca-based additives (CaO and MgO), which enhanced catalytic removal of PAHs and four fractions in petroleum from oily sludge at high temperature under an inert atmosphere (Liang et al., 2017; Lin et al., 2019).

The composite catalysts have attracted wide attention for their higher catalytic efficiencies than single-component metal oxides (Chen et al., 2022; Manviri Rani and Shanker, 2019). The recycled ferrous slags as mixtures of the above-mentioned active components have been explored in thermal catalysis and Fenton-like catalysis (Appendix A Table S5). In our study, the PAHs were completely removed from clay soil by thermal desorption using the catalyst of non-Ca-based titania-bearing blast furnace slag or Ca-based steel refining slag and the oxidant of air at the temperature of 350°C rather than strong oxidant of H₂O₂ in Fenton-like catalysis (Hu et al., 2019; Tsai and Kao, 2009). In addition, the Ca-based red mud mainly composed of Al₂O₃, Fe₂O₃, CaO and SiO₂ improved the thermal removal of PHs from sandy soil at the temperature of 400°C in N₂ (Liu et al., 2021).

3.3. Composites in emerging photo-thermal catalysis

Carbon-based materials (reduced graphene oxide (RGO) and N-doped carbon (NC)), metal chalcogenides (CdS and MoS₂), plasmonic metals (nano-Ag), tungsten oxides and bronze with localized surface plasmon resonance (LSPR) (WO_{3-x} and Cs_xWO₃) enable the transition metal oxides to highly efficiently adsorb solar energy and produce heat, which is vital to mitigate the foreshadowed global energy and environmental crisis (Appendix A Table S6). The RGO or NC can reduce recombination efficiency of photoinduced electron-hole pairs in single-phase black TiO₂ or CuO with narrow band gap by heterojunction formation (Chen et al., 2023; Zhu et al., 2021). Abundant sunlight can be adsorbed by RGO and black TiO₂ composites to provide heat for black TiO₂ with high concentration of Ti³⁺ and oxygen vacancy, and the oxidative removal efficiency of tetracycline is higher in this synergistic photo-thermal catalytic process than electrical heating catalysis (Zhu et al., 2021). Different from traditional heterojunction, a Z-scheme heterojunction can be formed between CdS quantum dots and ZnO_{1-x}TiO_{2-x}, between m-BiVO₄, t-BiVO₄ and Cs_{0.33}WO₃ to completely photothermal-catalytically degrade microplastics (bisphenol A), pesticide (2,6-dichlorophenol and 2,4,5-trichlorophenol) and antibiotic (tetracycline) into CO₂ and H₂O under visible and near-infrared light (Sun et al., 2020; Yang et al., 2023). The nanocrystal of Cs_xWO₃ can convert ultraviolet, visible and near-infrared light into local heat through LSPR absorption and small polaron absorption (Li et al., 2022; Yang et al., 2023). The TiO₂ coupled with both narrow band gap semiconductor of MoS₂ and LSPR material of nano-Ag in the ternary heterojunctions exhibited a strongest light adsorption and photothermal conversion, which raised central temperature of catalyst to 202°C within 1 min ((Zhao et al., 2019b) in Appendix A Table S6). The Fe₃O₄ coupled with LSPR material of WO_{3-x} and nano-Ag significantly strengthened photothermal catalytic-Fenton degradation of microplastics (bisphenol A) ((Liao et al., 2021) in Appendix A Table S6).

3.4. Alkaline compounds and reduction catalysts (nano-TiN and nZVI)

The additives such as CaO, Ca(OH)₂, NaOH, high f-CaO steel refining slag, metallic catalysts and nano-TiN are used to improve the degradation of persistent chlorinated organic contaminants, such as HCHs, DDTs, chlorophenol and PCBs (Appendix A Table S7). These catalytic reactions must be conducted under anoxic reductive conditions to avoid the production of highly toxic secondary contaminants such as polychlorinated dibenz-p-dioxins and polychlorinated dibenz-p-furans (PCDD/Fs) (Araújo et al., 2016; Zhao et al., 2017, 2019a).

In our study, the TD removal efficiency of PCBs from clay soil with PI of 32 was enhanced from 56.2% to 92.0% at a temperature of 250°C using 2% nano-metallic Fe (nZVI) or nano-TiN, which is higher than that using CaO or high f-CaO steel refining slag. The Ca(OH)₂ can effectively improve the TD efficiencies of PCBs from soil at temperatures of 400°C, but are less effective than metallic catalysts and NaOH (Liu et al., 2014, 2015a, 2019a). Ball milling can be used to drive highly exothermic solid-phase reactions between active mixtures of nano-metallic Ca- or Al-CaO and persistent chlorinated organic con-

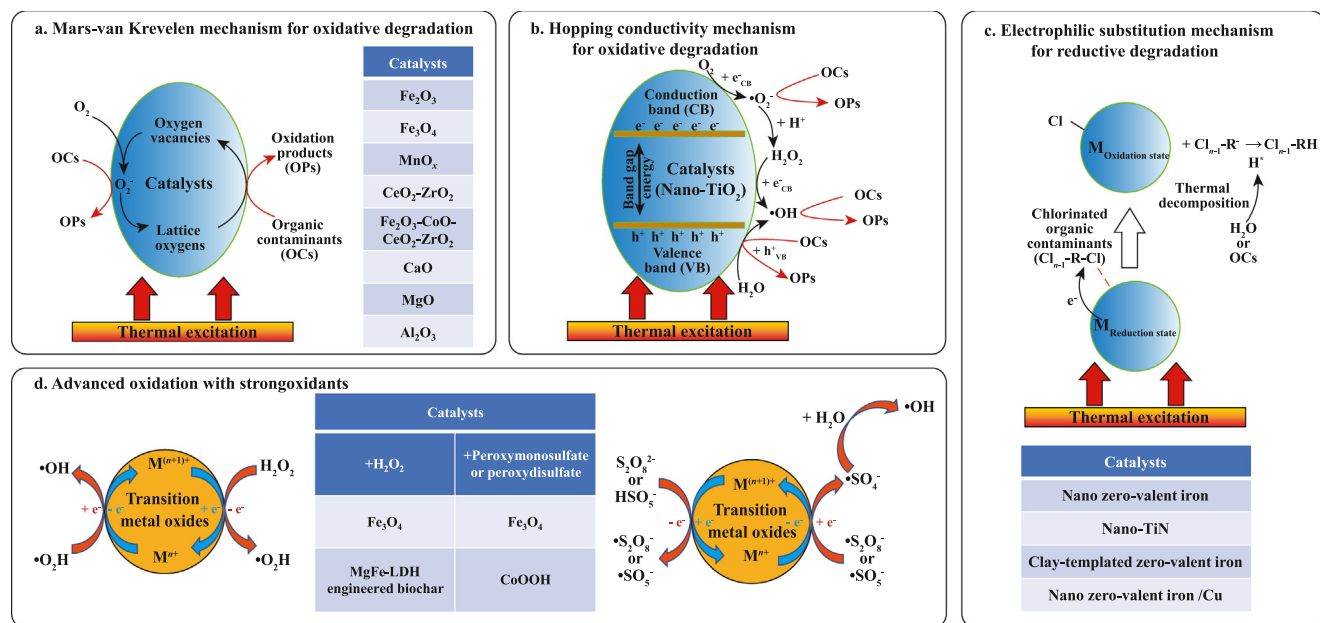


Fig. 3 – Possible mechanisms of thermal oxidative/reductive degradation of different organic contaminants as compared to chemical oxidation. (a) Mar-van Krevelen mechanism. (b) Hopping conductivity mechanism. (c) Electrophilic substitution mechanism. (d) Reactive radicals generated from strong oxidants that are harmful to human health. $\text{M}^{(n+1)+}$, high valence transition metals; M^{n+} , low valence transition metals.

taminants in solid-wastes and soil (Mallampati et al., 2014; Yu et al., 2020). In these reactions, CaO can inhibit the formation of HCl and the chlorophenols that are the vital precursors of PCDD/Fs (Deng et al., 2009; Wey et al., 2008). The nZVI has a standard potential of -440 mV (Elliott et al., 2009) and is used as a common reducing agent of PCBs and chlorpyrifos in soil and methanol/water due to its low cost, abundance, and environmentally-friendly properties (Appendix A Table S7). As compared to single nZVI, higher hydrodechlorination and removal efficiencies of PCB209 using clay supported nZVI were attributed to lower diameter and larger surface area as well as synergistic effects of active components in clay and nZVI, same as bimetallic nZVI/Cu (Graça et al., 2020; Yu et al., 2016).

4. Mechanisms of catalytic additives

4.1. Possible mechanisms of thermal catalysis

There are Mars-van Krevelen (also called MvK Fig. 3a) and hopping conductivity mechanisms (Fig. 3b) for the thermal catalysis and oxidative degradation of nonchlorinated organic contaminants, and electrophilic substitution (Fig. 3c) for the reductive degradation of chlorinated organic contaminants. For the MvK mechanism (Fig. 3a), the lattice oxygens, defined as unstable bulk phase oxygen that forms the crystal structure of metal oxide catalysts are activated by thermal excitation, which directly oxidize organic contaminants and generate oxygen vacancies on the surfaces of the oxides (step 1: reduction of the catalyst) (Chen et al., 2019; Gao et al., 2023; Mars and van Krevelen, 1954). The superoxide anion

radical (O_2^-) which is generated through the adsorption of O_2 from the atmosphere onto oxygen vacancies in the catalysts and activation by the electrons released from adjacent metal ions, reacts with the organic contaminants and regenerates lattice oxygens to fill the oxygen vacancies (step 2: re-oxidation of the catalyst) (Kwon et al., 2018). The amounts of oxygen vacancies and the catalytic activities can be improved by pre-reduction of the transition metal oxides or metal doping (Gao et al., 2023; Ge et al., 2022; Widmann and Behm, 2018). Through this mechanism, PHs and PAHs can be catalytically oxidized by Fe_2O_3 (Liu et al., 2020), Fe_3O_4 (Oden et al., 2022), MnO_x (Cheng et al., 2022; Oden et al., 2022; Wang et al., 2020), $\text{CeO}_2\text{-ZrO}_2$ (Ajumobi et al., 2018), $\text{Fe}_2\text{O}_3\text{-CoO-CeO}_2\text{-ZrO}_2$ (Ajumobi et al., 2018) and mixture of Ca/Mg/Al oxides (Liang et al., 2017; Liu et al., 2021).

Through a hopping conductivity mechanism (Fig. 3b), TiO_2 can catalyze and oxidize the petroleum contaminants in oily sludge (Dang et al., 2021) and polycarbonate in used optical disks (Shinbara et al., 2005). The electrons occupying the valance band (VB) that is the outermost electron orbital of transition-metal oxides are excited over relatively lower barriers to the lowest unoccupied conduction band (CB) under heating mode, and thermally generated electron (e^-_{CB} at conduction band) and hole (h^+_{VB} at valance band) pairs are obtained (Chen et al., 2019; Dang et al., 2021; Wan et al., 2019). The $\cdot\text{OH}$ and H^+ are generated from the h^+_{VB} -induced dissociation of H_2O on the surface of catalysts, while the $\cdot\text{O}_2^-$ with a standard electrode potential of 2.4 V is generated from the e^-_{CB} -induced reduction of dissolved oxygen at the CB (Dang et al., 2021; Wan et al., 2019). The generated $\cdot\text{O}_2^-$ reacts with H^+ from dissociation of H_2O to obtain intermediate product of H_2O_2 , which further reacts with e^-_{CB} at conduction band to

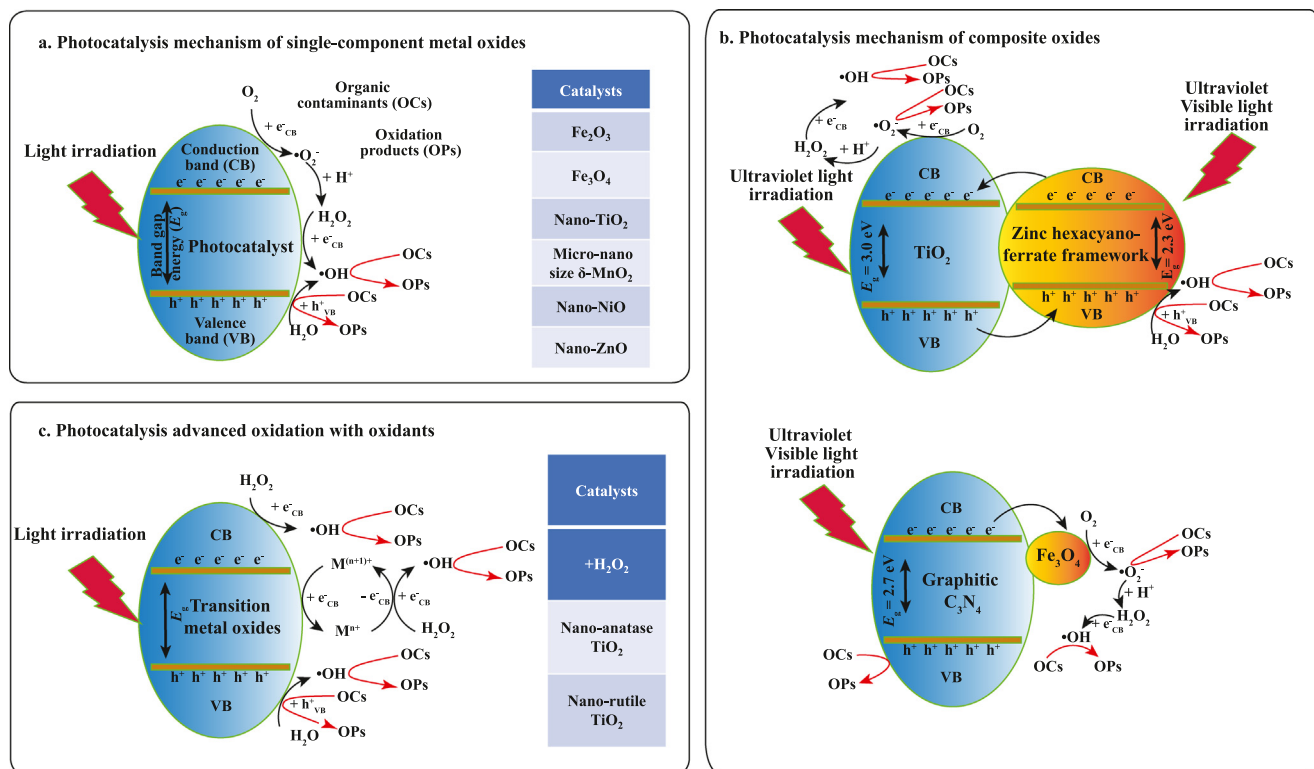


Fig. 4 – Generation process of reactive oxidative radicals and oxidative degradation of nonchlorinated organic contaminants in photocatalysis. (a) Photocatalysis mechanism of single-component metal oxides. (b) Photocatalysis mechanism of composite oxides. (c) Photocatalysis advanced oxidation with oxidants.

generate highly reactive •OH with a standard electrode potential of 2.8 V (Jorfi et al., 2018; Shinde et al., 2013). Organic contaminants are directly oxidized by electron holes (h⁺_{VB}) at valance band or indirectly oxidized by the oxygen free radicals of •OH and •O₂⁻ that are generated from H₂O and O₂ following the steps discussed above (Dang et al., 2021; Davis et al., 2020; Shinbara et al., 2005; Wan et al., 2019).

Electrophilic substitution, the main reductive dechlorination mechanism of chlorinated organic contaminants (R-Cl), is shown in Fig. 3c. The dissociative adsorption of the Cl atom of R-Cl on the metal element in the form of the reduction state (M_{Reduction state}) and other electrophilic catalysts, is coupled with the electron withdrawing of the C atom of R-Cl, resulting in cleavage of the C-Cl bond and formation of the metal-Cl bond in the form of the oxidation state (M_{Oxidation state}) (Davis et al., 2020; Liu et al., 2014, 2015b; Su et al., 2015). And then the H^{*} (hydrogen donor) from the thermocatalytic dissociation of H₂O or decomposition of organic contaminants reacts with R⁻ and generates R-H (Liu et al., 2019b; Su et al., 2015). Through this mechanism, PCBs in soil and soil slurry (Liu et al., 2014; Yu et al., 2016), and chlorpyrifos in methanol/water (Graça et al., 2020) are catalyzed and reduced by nano-TiN, nano-metallic Fe and bimetallic nZVI/Cu. Moreover, NaOH and Ca(OH)₂, two types of alkali, facilitate the dechlorination of R-Cl by weakening the C-Cl bond (Liu et al., 2015b, 2019b). Benzene rings of organic contaminants can be further reduced into cyclohexane rings and then decomposed into lower molecular weight alkanes and alkenes (Nomura et al., 2005, 2012).

Instead of thermal excitation, the radical oxygen species can be produced by strong oxidant H₂O₂, peroxydisulfate and peroxymonosulfate involved in the cycles of high- and low-valence transition metals (M⁽ⁿ⁺¹⁾⁺ and Mⁿ⁺) in a Fenton-like or photo-Fenton-like reaction of PHs, PAHs or antibiotics contaminated soil (Fig. 3d). With transition metal oxide possessing multiple valences such as Fe₃O₄ (FeO-Fe₂O₃) (Biache et al., 2015b; Boulangé et al., 2019; Mirzaee et al., 2017) and MgFe-LDH engineered biochar composites containing Fe₃O₄ (Chen et al., 2022), the H₂O₂ is activated and oxidized to generate •O₂H, and finally to generate •OH with stronger oxidability (Tao et al., 2021). Similarly, S₂O₈²⁻ and HSO₅⁻ can be activated by Fe₃O₄ (Usman et al., 2012), non-stoichiometric cobalt oxyhydroxide (CoOOH) where cobalt generally has either Co³⁺ or Co⁴⁺ oxidation states (Lyu et al., 2019) to generate •OH and •SO₄⁻ ($E^{\circ} = 2.6$ V) (Jaafarzadeh et al., 2017; Zhai et al., 2019; Zhu et al., 2017). However, these chemical oxidants would cause skin burns, eye damage and respiratory irritation (Mirzaee et al., 2017; Usman et al., 2012).

4.2. Possible mechanisms of photocatalysis against thermal catalysis

The photocatalysis has attracted wide attention as a green technology independent of heat released by fuel energy (Fig. 4). The single component homogeneous catalysts, including Fe₂O₃ (Marquès et al., 2020; Wang et al., 2009; Zhang et al., 2006), Fe₃O₄ (Luo et al., 2018), TiO₂ (Chang Chien et al., 2011b; Eker and Hatipoglu, 2019; Silva et al., 2020; Wang et al.,

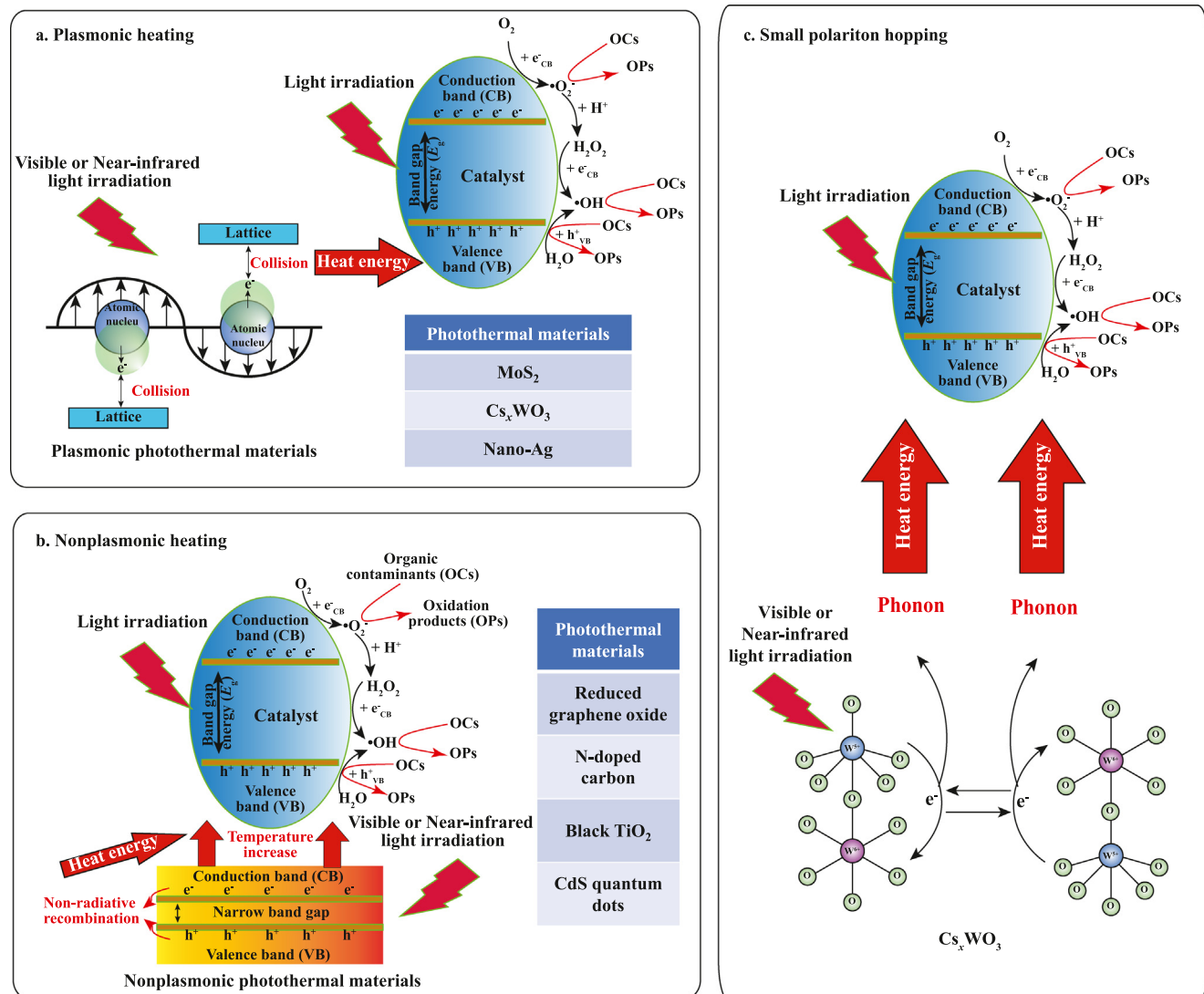


Fig. 5 – Photo-heat conversion and oxidative removal mechanisms of nonchlorinated organic contaminants in synergistic photo-thermal-catalysis. (a) Plasmonic heating. (b) Nonplasmonic heating. (c) Small polariton hopping.

2016; Zhang et al., 2006, 2008), micro-nano size δ -MnO₂ (Chang Chien et al., 2011a), nano-NiO (Sliem et al., 2019) and nano-ZnO (Sliem et al., 2019) are initiated by the light energy ($h\nu$) corresponding to or higher than the band gap energy (E_g) between VB and CB (Fig. 4a), similar to the hopping conductivity mechanism of thermal catalysis (Fig. 3b). The heterogeneous composite catalysts, such as nano-Fe₃O₄ coated graphitic C₃N₄ (Wang et al., 2019b), TiO₂ based zinc hexacyanoferrate framework nanocomposite (Manviri Rani and Shanker, 2019), and Fe₃O₄/SiO₂/TiO₂ composites (Xu et al., 2011) adsorb both UV light and visible light (Fig. 4b). The photogenerated e⁻_{CB} and h⁺_{VB} pairs transferred between two dissimilar photocatalysts through the heterojunction formed at their interface, while it is difficult to generate •OH for the h⁺_{VB} on the surfaces of graphitic C₃N₄ with lower CB energy level than •OH (Manviri Rani and Shanker, 2019; Wang et al., 2019b). The recombination of the e⁻_{CB} and h⁺_{VB} pair is inhibited due to spatial separation, resulting in prolonged lifetimes and enhanced photocatalysis efficiency (Li et al., 2015; Nguyen-

Phan et al., 2016). In photocatalysis/H₂O₂ synergistic reaction (Fig. 4c), the photogenerated electrons at the surface of catalysts were involved in the M^{(n+1)/Mⁿ⁺ cycle and converted oxidants into •OH (Dong et al., 2010a, 2010b; Gu et al., 2012), along with the oxidants and H₂O were activated by photogenerated e⁻_{CB} and h⁺_{VB} (Fabbri et al., 2008; Jaafarzadeh et al., 2017; Mandal et al., 2019; Zhang et al., 2019). These processes were similar as hopping conductivity mechanism of thermal catalysis combined with Fenton-like catalysis (Fig. 3b and d).}

4.3. Mechanisms of synergistic photo-thermal-catalysis

The mechanisms of plasmonic heating (Fig. 5a), nonplasmonic heating (Fig. 5b) and small-polaron hopping (Fig. 5c) could shed some light on highly efficient and environmental-friendly synergistic photo-thermal-catalysis. The plasmonic photothermal materials (Fig. 5a) including MoS₂ (Zhao et al., 2019b), Cs_xWO₃ (Li et al., 2022; Yang et al., 2023), and nano-Ag (Liao et al., 2021; Zhao et al., 2019b) convert the light energy

to heat energy through LSPR. When the frequency of incident light matches the frequency of valence electrons oscillating against the restoring force of atomic nucleus that is defined as the force responsible for pushing the mass back toward its equilibrium position, the collective electron resonance (also called plasmon) was induced by resonant photons (Linic et al., 2015; Wang and Astruc, 2014). These excited electrons or plasmons are relaxed by colliding with the lattice of plasmonic materials, which generated and transferred heat to catalysts through phonon-phonon (discrete units or quantum of vibrational energy) coupling (Bisoyi et al., 2018). And then, the catalysts are initiated by both light energy and generated heat energy, similar to the hopping conductivity mechanism of thermal catalysis (Fig. 3b).

The nonplasmonic photothermal materials (Fig. 5b) have a narrow band gap, including reduced graphene oxide (Zhu et al., 2021), N-doped carbon (Chen et al., 2023), black TiO₂ (Zhu et al., 2021) and CdS quantum dots (Sun et al., 2020). After excitation by visible/near-infrared light, the non-radiative recombination (also called auger recombination) of e⁻_{CB} and h⁺_{VB} releases phonons with higher energy instead of photons (the radiative recombination), and then heat energy is released via electron-phonon coupling (coupling of itinerant electrons to lattice vibrations transferring energy from hot electrons to the atomic vibrations) and phonon-phonon coupling which increases the temperature of the reaction system (Li et al., 2019; Zhang et al., 2021b). The small-polaron hopping instead of large polarons (electrons or holes) excitation is another photothermal conversion mechanism of Cs_xWO₃ through the cycle of W⁵⁺/W⁶⁺ due to the electron delocalized over both adjacent sites (Fig. 5c). After visible/near-infrared light irradiation, the W⁵⁺ was excited to generate W⁶⁺ and electrons, the electrons reacted with the adjacent W to form a new W⁵⁺ site and phonons, along with heat transferring and catalytical oxidization of antibiotic (tetracycline) and microplastics (bisphenol A) as emerging POPs (Li et al., 2022; Yang et al., 2023).

5. Conclusions

In order to alleviate agglomeration and reduce the fuel energy consumption in the thermal removal of recalcitrant POPs from clay soil, this paper reviewed soil conditioners and catalysts. CaO/Ca(OH)₂ as Ca-based soil conditioners for smectite or montmorillonite, were differentiated from MgO/Mg(OH)₂ and SiO₂ as non-Ca-based soil conditioners for kaolin clay and lower plastic clay. Reutilization of Ca-based slags and fly ashes containing multiple active components can reduce soil plasticity, which can be controlled using alkaline auxiliary additives. The plasticity and agglomeration of clay soil can be reduced through cation exchange and flocculation. The oxides of transition metals (Fe, Ti, Mn, Co, Zr, Ni and Zn), the Ca-based and non-Ca-based alkali/alkaline earth metal (hydrated)oxides and carbonates, and their composites are effective oxidizing additives for catalytically degrading POPs without strong chemical oxidants through the Mars-van Krevelen and hopping conductivity mechanisms. Moreover, synergistic photo-thermal-catalysis is more highly efficient and environmentally-friendly through mechanisms of nonplas-

monic heating, plasmonic heating and small polariton hopping. Additives such as CaO, NaOH, nZVI and nano-TiN were discussed for catalytical reduction of chlorinated organic contaminants through an electrophilic substitution mechanism.

Declaration of Competing Interest

The authors declare that they have no known competing financial interests or personal relationships that could have appeared to influence the work reported in this paper.

Acknowledgments

This work was supported by the National Key R&D Program of China (No. 2018YFC1802101); and the National Natural Science Foundation of China (No. 52170149).

Appendix A Supplementary data

Supplementary material associated with this article can be found, in the online version, at doi:10.1016/j.jes.2023.11.006.

REFERENCES

- Ajumobi, O.O., Muraza, O., Kondoh, H., Hasegawa, N., Nakasaka, Y., Yoshikawa, T., et al., 2018. Upgrading oil sand bitumen under superheated steam over ceria-based nanocomposite catalysts. *Appl. Energ.* 218, 1–9.
- Al-Mukhtar, M., Lasledj, A., Alcover, J.F., 2010. Behaviour and mineralogy changes in lime-treated expansive soil at 20°C. *Appl. Clay Sci.* 50, 191–198.
- Amundson, R., Berhe Asmeret, A., Hopmans Jan, W., Olson, C., Sztein, A.E., Sparks Donald, L., 2015. Soil and human security in the 21st century. *Science* 348, 1261071.
- Araújo, M.M., Ignatius, S.G., Oliveira, A.O., Oliveira, S.S., Ferttonani, F.L., Paste, I.A., 2016. Thermal desorption of HCH. *J. Therm. Anal. Calorim.* 123, 1019–1029.
- Barker, J.E., Rogers, C.D., Boardman, D.I., 2006. Physio-chemical changes in clay caused by ion migration from lime piles. *J. Mater. Civ. Eng.* 18, 182–189.
- Biache, C., Lorgeoux, C., Saada, A., Faure, P., 2015a. Behavior of PAH/mineral associations during thermodesorption: Impact for the determination of mineral retention properties towards PAHs. *Anal. Bioanal. Chem.* 407, 3509–3516.
- Biache, C., Lorgeoux, C., Andriatsiharoana, S., Colombano, S., Faure, P., 2015b. Effect of pre-heating on the chemical oxidation efficiency: implications for the PAH availability measurement in contaminated soils. *J. Hazard. Mater.* 286, 55–63.
- Bisoyi, H.K., Urbas, A.M., Li, Q., 2018. Soft materials driven by photothermal effect and their applications. *Adv. Opt. Mater.* 6, 1800458.
- Boulangé, M., Lorgeoux, C., Biache, C., Saada, A., Faure, P., 2019. Fenton-like and potassium permanganate oxidations of PAH-contaminated soils: impact of oxidant doses on PAH and polar PAC (polycyclic aromatic compound) behavior. *Chemosphere* 224, 437–444.
- Buazar, F., 2019. Impact of biocompatible nanosilica on green stabilization of subgrade soil. *Sci. Rep.* 9, 15147.
- Budhu, M., 2010. *Soil Mechanics and Foundations*. John Wiley & Sons, Inc., New York.

- Cassidy, D.P., Srivastava, V.J., Dombrowski, F.J., Lingle, J.W., 2015. Combining *in situ* chemical oxidation, stabilization, and anaerobic bioremediation in a single application to reduce contaminant mass and leachability in soil. *J. Hazard. Mater.* 297, 347–355.
- Chang Chien, S.W., Chang, C.H., Chen, S.H., Wang, M.C., Madhava Rao, M., Satya Veni, S., 2011a. Oxidative degradation of pyrene in contaminated soils by δ -MnO₂ with or without sunlight irradiation. *Sci. Total Environ.* 409, 4078–4086.
- Chang Chien, S.W., Chang, C.H., Chen, S.H., Wang, M.C., Madhava Rao, M., Satya Veni, S., 2011b. Effect of sunlight irradiation on photocatalytic pyrene degradation in contaminated soils by micro-nano size TiO₂. *Sci. Total Environ.* 409, 4101–4108.
- Chen, H., Ku, J., Wang, L., 2019. Thermal catalysis under dark ambient conditions in environmental remediation: fundamental principles, development, and challenges. *Chin. J. Catal.* 40, 1117–1134.
- Chen, Q., Cheng, Z., Li, X., Wang, C., Yan, L., Shen, G., et al., 2022. Degradation mechanism and QSAR models of antibiotic contaminants in soil by MgFe-LDH engineered biochar activating urea-hydrogen peroxide. *Appl. Catal. B: Environ.* 302, 120866.
- Chen, W., Chen, M., Sun, C., Chen, T., Chen, Z., Ji, L., et al., 2020a. Eggshell and plant ash addition during the thermal desorption of polycyclic aromatic hydrocarbon-contaminated coke soil for improved removal efficiency and soil quality. *Environ. Sci. Pollut. Res.* 27, 11050–11065.
- Chen, Y., Dai, Y., Li, Y., Hou, Z., Gao, B., Yue, Q., et al., 2023. Oxygen vacancies-mediated CuO@N-doped carbon nanocomposites for non-radical-dominated photothermal catalytic degradation of contaminants. *J. Clean. Prod.* 389, 136054.
- Chen, Z., Zhang, Z., Liu, D., Chi, X., Chen, W., Chi, R., 2020b. Swelling of clay minerals during the leaching process of weathered crust elution-deposited rare earth ores by magnesium salts. *Powder Technol.* 367, 889–900.
- Cheng, P., Lin, Z., Zhao, X., Waigi, M.G., Vasilyeva, G.K., Gao, Y., 2022. Enhanced transformation capability towards benzo(a)pyrene by Fe(III)-modified manganese oxides. *J. Hazard. Mater.* 431, 128637.
- Cheng, Y., Sun, H., Yang, E., Lv, J., Wen, B., Sun, F., et al., 2021. Distribution and bioaccessibility of polycyclic aromatic hydrocarbons in industrially contaminated site soils as affected by thermal treatment. *J. Hazard. Mater.* 411, 125129.
- Cheshomi, A., Eshaghi, A., Hassanpour, J., 2017. Effect of lime and fly ash on swelling percentage and Atterberg limits of sulfate-bearing clay. *Appl. Clay Sci.* 135, 190–198.
- Dai, W.J., Wu, P., Liu, D., Hu, J., Cao, Y., Liu, T.Z., et al., 2020. Adsorption of polycyclic aromatic hydrocarbons from aqueous solution by organic montmorillonite sodium alginate nanocomposites. *Chemosphere* 251, 126074.
- Dang, Z., Zhu, X., Wang, L., Ji, G., 2021. Titanium dioxide catalytic hydrothermal liquefaction to treat oily sludge: as hydrogen production catalyst. *Chem. Eng. J. Adv.* 8, 100139.
- Dash, S.K., Hussain, M., 2012. Lime stabilization of soils: reappraisal. *J. Mater. Civ. Eng.* 24, 707–714.
- Davin, M., Colinet, G., Fauconnier, M.L., 2021. Targeting the right parameters in PAH remediation studies. *Environ. Pollut.* 278, 116857.
- Davis, R.J., Liljestrand, H.M., Katz, L.E., 2020. Evidence for multiple removal pathways in low-temperature (200–400 °C) thermal treatment of pentachlorophenol-laden soils. *J. Hazard. Mater.* 400, 122870.
- Deng, W., Yan, J., Li, X., Wang, F., Chi, Y., Lu, S., 2009. Emission characteristics of dioxins, furans and polycyclic aromatic hydrocarbons during fluidized-bed combustion of sewage sludge. *J. Environ. Sci.* 21, 1747–1752.
- Dong, D., Li, P., Li, X., Zhao, Q., Zhang, Y., Jia, C., et al., 2010a. Investigation on the photocatalytic degradation of pyrene on soil surfaces using nanometer anatase TiO₂ under UV irradiation. *J. Hazard. Mater.* 174, 859–863.
- Dong, D., Li, P., Li, X., Xu, C., Gong, D., Zhang, Y., et al., 2010b. Photocatalytic degradation of phenanthrene and pyrene on soil surfaces in the presence of nanometer rutile TiO₂ under UV-irradiation. *Chem. Eng. J.* 158, 378–383.
- Eker, G., Hatipoglu, M., 2019. Effect of UV wavelength, temperature and photocatalyst on the removal of PAHs from industrial soil with photodegradation applications. *Environ. Technol.* 40, 3793–3803.
- Elert, K., Nieto, F., Azañón, J.M., 2017. Effects of lime treatments on marls. *Appl. Clay Sci.* 135, 611–619.
- Elliott, D.W., Lien, H.L., Zhang, W.X., 2009. Degradation of lindane by zero-valent iron nanoparticles. *J. Environ. Eng.* 135, 317–324.
- EEA (European Environment Agency), 2020. EEA signals 2020 — towards zero pollution in Europe. <https://www.eea.europa.eu/publications/signals-2020>.
- Fabbri, D., Prevot, A.B., Zelano, V., Ginepro, M., Pramauro, E., 2008. Removal and degradation of aromatic compounds from a highly polluted site by coupling soil washing with photocatalysis. *Chemosphere* 71, 59–65.
- Falciglia, P.P., De Guidi, G., Catalfo, A., Vagliasindi, F.G.A., 2016. Remediation of soils contaminated with PAHs and nitro-PAHs using microwave irradiation. *Chem. Eng. J.* 296, 162–172.
- Falciglia, P.P., Giustra, M.G., Vagliasindi, F.G.A., 2011a. Low-temperature thermal desorption of diesel polluted soil: influence of temperature and soil texture on contaminant removal kinetics. *J. Hazard. Mater.* 185, 392–400.
- Falciglia, P.P., Giustra, M.G., Vagliasindi, F.G.A., 2011b. Soil texture affects adsorption capacity and removal efficiency of contaminants in *ex situ* remediation by thermal desorption of diesel-contaminated soils. *Chem. Ecol.* 27, 119–130.
- Feng, J., Sun, J., 2020. A comparison of the 10-year properties of converter steel slag activated by high temperature and an alkaline activator. *Constr. Build. Mater.* 234, 116948.
- Gao, W., Tang, X., Yi, H., Jiang, S., Yu, Q., Xie, X., et al., 2023. Mesoporous molecular sieve-based materials for catalytic oxidation of VOC: A review. *J. Environ. Sci.* 125, 112–134.
- Ge, H., Kuwahara, Y., Yamashita, H., 2022. Development of defective molybdenum oxides for photocatalysis, thermal catalysis, and photothermal catalysis. *Chem. Commun.* 58, 8466–8479.
- Goodarzi, A.R., Salimi, M., 2015. Stabilization treatment of a dispersive clayey soil using granulated blast furnace slag and basic oxygen furnace slag. *Appl. Clay Sci.* 108, 61–69.
- Graça, C.A.L., Mendes, M.A., Teixeira, A.C.S.C., Correia de Veloso, A., 2020. Anoxic degradation of chlorpyrifos by zerovalent monometallic and bimetallic particles in solution. *Chemosphere* 244, 125461.
- Gu, J., Dong, D., Kong, L., Zheng, Y., Li, X., 2012. Photocatalytic degradation of phenanthrene on soil surfaces in the presence of nanometer anatase TiO₂ under UV-light. *J. Environ. Sci.* 24, 2122–2126.
- Han, Z., Jiao, W., Tian, Y., Hu, J., Han, D., 2020. Lab-scale removal of PAHs in contaminated soil using electrical resistance heating: Removal efficiency and alteration of soil properties. *Chemosphere* 239, 124496.
- He, L., Sang, Y., Yu, W., Li, W., Jiao, Y., Ma, F., et al., 2020. Polymerization and carbonization behaviors of 2-methylnaphthalene in contaminated soil during thermal desorption. *Water Air Soil Poll.* 231, 505.
- Hu, E., He, Z., Nan, X., Yuan, Z., Li, X., 2019. Removal of phenanthrene and pyrene from contaminated sandy soil using hydrogen peroxide oxidation catalyzed by basic oxygen furnace slag. *Environ. Sci. Pollut. Res.* 26, 9281–9292.
- Jaafarzadeh, N., Ghanbari, F., Ahmadi, M., 2017. Catalytic degradation of 2,4-dichlorophenoxyacetic acid (2,4-D) by

- nano- Fe_2O_3 activated peroxymonosulfate: Influential factors and mechanism determination. *Chemosphere* 169, 568–576.
- Jafer, H., Atherton, W., Sadique, M., Ruddock, F., Loffill, E., 2018. Stabilisation of soft soil using binary blending of high calcium fly ash and palm oil fuel ash. *Appl. Clay Sci.* 152, 323–332.
- Jeon, S.B., Kim, M.C., Cho, J.H., Jung, J.H., Oh, K.J., 2013. Desorption kinetics of polycyclic aromatic hydrocarbons in soil using lab-scale rotary desorber. *Korean J. Chem. Eng.* 30, 1896–1903.
- Jia, H., Zhao, J., Fan, X., Dilimulati, K., Wang, C., 2012. Photodegradation of phenanthrene on cation-modified clays under visible light. *Appl. Catal. B: Environ.* 123–124, 43–51.
- Jorfi, S., Pourfadakari, S., Kakavandi, B., 2018. A new approach in sono-photocatalytic degradation of recalcitrant textile wastewater using $\text{MgO}@\text{Zeolite}$ nanostructure under UVA irradiation. *Chem. Eng. J.* 343, 95–107.
- Kalhor, A., Ghazavi, M., Roustaei, M., Mirhosseini, S.M., 2019. Influence of nano- SiO_2 on geotechnical properties of fine soils subjected to freeze-thaw cycles. *Cold Reg. Sci. Technol.* 161, 129–136.
- Karaca, G., Baskaya, H.S., Tasdemir, Y., 2016. Removal of polycyclic aromatic hydrocarbons (PAHs) from inorganic clay mineral: Bentonite. *Environ. Sci. Pollut. Res.* 23, 242–252.
- Kwon, S., Deshlahra, P., Iglesia, E., 2018. Dioxygen activation routes in Mars-van Krevelen redox cycles catalyzed by metal oxides. *J. Catal.* 364, 228–247.
- Li, F., Zhang, Y., Wang, S., Li, G., Yue, X., Zhong, D., et al., 2020. Insight into ex-situ thermal desorption of soils contaminated with petroleum via carbon number-based fraction approach. *Chem. Eng. J.* 385, 123946.
- Li, K., Gao, S., Wang, Q., Xu, H., Wang, Z., Huang, B., et al., 2015. In-situ-reduced synthesis of Ti^{3+} self-doped $\text{TiO}_2/\text{g-C}_3\text{N}_4$ heterojunctions with high photocatalytic performance under LED light irradiation. *ACS Appl. Mater. Interfaces* 7, 9023–9030.
- Li, G., Guo, S., Hu, J., 2016. The influence of clay minerals and surfactants on hydrocarbon removal during the washing of petroleum-contaminated soil. *Chem. Eng.* 286, 191–197.
- Li, J.J., Cai, S.C., Chen, X., Yan, D.X., Chen, J., Jia, H.P., 2019. Engineering rGO nanosheets-adsorption layer supported Pt nanoparticles to enhance photo-thermal catalytic activity under light irradiation. *J. Mater. Chem. A* 7, 11985–11995.
- Li, T., Liu, J., Shi, F., Song, X., Zhang, H., Zhang, H., et al., 2022. Construction of a novel highly porous $\text{BiOBr}/\text{Cs}_x\text{WO}_3@\text{SiO}_2$ composite aerogel: adsorption/self-heating photocatalytic synergistic degradation of antibiotics and mechanism study. *J. Environ. Chem. Eng.* 10, 107785.
- Liang, P., Yu, J., Zhang, Y., Jiao, T., Qin, X., 2017. Effects of natural dolomite catalysts on cracking anthracene oil. *Energ. Fuel.* 31, 11765–11772.
- Liao, J., Xu, Y., Zhao, Y., Wang, C.C., Ge, C., 2021. Ag and Fe_3O_4 comodified WO_{3-x} nanocomposites for catalytic photothermal degradation of pharmaceuticals and personal care products. *ACS Appl. Nano Mater.* 4, 1898–1905.
- Lin, B., Huang, Q., Ali, M., Wang, F., Chi, Y., Yan, J., 2019. Continuous catalytic pyrolysis of oily sludge using U-shape reactor for producing saturates-enriched light oil. *Proc. Combust. Inst.* 37, 3101–3108.
- Lin, B., Wang, J., Huang, Q., Chi, Y., 2017. Effects of potassium hydroxide on the catalytic pyrolysis of oily sludge for high-quality oil product. *Fuel* 200, 124–133.
- Linic, S., Aslam, U., Boerigter, C., Morabito, M., 2015. Photochemical transformations on plasmonic metal nanoparticles. *Nat. Mater.* 14, 567–576.
- Liu, B., Niu, W., Hu, X., Liu, F., Jiang, J., Wang, H., et al., 2022. Enhanced oxidative activation of chlorine dioxide by divalent manganese ion for efficient removal of PAHs in industrial soil. *Chem. Eng. J.* 434, 134631.
- Liu, H., Li, J., Zhao, M., Li, Y., Chen, Y., 2019a. Remediation of oil-based drill cuttings using low-temperature thermal desorption: performance and kinetics modeling. *Chemosphere* 235, 1081–1088.
- Liu, J., Chen, T., Qi, Z., Yan, J., Buekens, A., Li, X., 2014. Thermal desorption of PCBs from contaminated soil using nano zerovalent iron. *Environ. Sci. Pollut. Res.* 21, 12739–12746.
- Liu, J., Qi, Z., Zhao, Z., Li, X., Buekens, A., Yan, J., et al., 2015a. Thermal desorption of PCB-contaminated soil with sodium hydroxide. *Environ. Sci. Pollut. Res.* 22, 19538–19545.
- Liu, J., Qi, Z., Li, X., Chen, T., Buekens, A., Yan, J., et al., 2015b. Thermal desorption of PCBs from contaminated soil with copper dichloride. *Environ. Sci. Pollut. Res.* 22, 19093–19100.
- Liu, J., Zhang, H., Yao, Z., Li, X., Tang, J., 2019b. Thermal desorption of PCBs contaminated soil with calcium hydroxide in a rotary kiln. *Chemosphere* 220, 1041–1046.
- Liu, Y., Li, X., Zhang, W., Ma, F., Zhang, Q., Gu, Q., 2021. Pyrolysis of heavy hydrocarbons in weathered petroleum-contaminated soil enhanced with inexpensive additives at low temperatures. *J. Clean. Prod.* 302, 127017.
- Liu, Y., Zhang, Q., Wu, B., Li, X., Ma, F., Li, F., et al., 2020. Hematite-facilitated pyrolysis: An innovative method for remediating soils contaminated with heavy hydrocarbons. *J. Hazard. Mater.* 383, 121165.
- Luo, Z., Min, Y., Qu, L., Song, Y., Hong, Y., 2021. Remediation of phenanthrene contaminated soil by ferrous oxalate and its phytotoxicity evaluation. *Chemosphere* 265, 129070.
- Luo, Z., Wang, J., Song, Y., Zheng, X., Qu, L., Wu, Z., et al., 2018. Remediation of phenanthrene contaminated soil by a solid state photo-Fenton reagent based on mesoporous magnetite/carboxylate-rich carbon composites and its phytotoxicity evaluation. *ACS Sustain. Chem. Eng.* 6, 13262–13275.
- Lyu, C., He, D., Chang, Y., Zhang, Q., Wen, F., Wang, X., 2019. Cobalt oxyhydroxide as an efficient heterogeneous catalyst of peroxymonosulfate activation for oil-contaminated soil remediation. *Sci. Total Environ.* 680, 61–69.
- Mallampati, S.R., Mitoma, Y., Okuda, T., Sakita, S., Simion, C., 2014. Simultaneous decontamination of cross-polluted soils with heavy metals and PCBs using a nano-metallic Ca/CaO dispersion mixture. *Environ. Sci. Pollut. Res.* 21, 9270–9277.
- Mandal, S., Adhikari, S., Pu, S., Wang, X., Kim, D.H., Patel, R.K., 2019. Interactive $\text{Fe}_2\text{O}_3/\text{porous SiO}_2$ nanospheres for photocatalytic degradation of organic pollutants: kinetic and mechanistic approach. *Chemosphere* 234, 596–607.
- Manviri Rani, R., Shanker, U., 2019. Degradation of tricyclic polycyclic aromatic hydrocarbons in water, soil and river sediment with a novel TiO_2 based heterogeneous nanocomposite. *J. Environ. Manag.* 248, 109340.
- Marquès, M., Cervelló, D., Mari, M., Sierra, J., Schuhmacher, M., Domingo, J.L., et al., 2020. The role of iron oxide on the photodegradation of polycyclic aromatic hydrocarbons: characterization and toxicity. *Polycycl. Aromat. Compd.* 40, 524–534.
- Mars, P., van Krevelen, D.W., 1954. Oxidations carried out by means of vanadium oxide catalysts. *Chem. Eng. Sci.* 3, 41–59.
- MEE (Ministry of Ecology and Environment of the P.R. China), 2014. Report on the national general survey of soil contamination. https://www.mee.gov.cn/gkml/stbjgw/qt/201404/t20140417_270670.htm.
- Mirzaee, E., Gitipour, S., Mousavi, M., Amini, S., 2017. Optimization of total petroleum hydrocarbons removal from Mahshahr contaminated soil using magnetite nanoparticle catalyzed Fenton-like oxidation. *Environ. Earth Sci.* 76, 165.
- Modarres, A., Nosoudy, Y.M., 2015. Clay stabilization using coal waste and lime — technical and environmental impacts. *Appl. Clay Sci.* 116–117, 281–288.
- Nguyen-Phan, T.D., Luo, S., Vovchok, D., Llorca, J., Graciani, J., Sanz, J.F., et al., 2016. Visible light-driven H_2 production over

- highly dispersed ruthenia on rutile TiO₂ nanorods. *ACS Catal.* 6, 407–417.
- Nomura, Y., Fujiwara, K., Terada, A., Nakai, S., Hosomi, M., 2012. Mechanochemical degradation of γ -hexachlorocyclohexane by a planetary ball mill in the presence of CaO. *Chemosphere* 86, 228–234.
- Nomura, Y., Nakai, S., Hosomi, M., 2005. Elucidation of degradation mechanism of dioxins during mechanochemical treatment. *Environ. Sci. Technol.* 39, 3799–3804.
- O'Brien, P.L., DeSutter, T.M., Casey, F.X.M., Khan, E., Wick, A.F., 2018. Thermal remediation alters soil properties – a review. *J. Environ. Manag.* 206, 826–835.
- Oden, C.P., Werth, C.J., Notini, L., Katz, L.E., 2022. Fate of pyrene on mineral surfaces during thermal remediation as a function of temperature. *Environ. Sci.: Processes Impacts* 24, 1181–1194.
- Ossai, I.C., Ahmed, A., Hassan, A., Hamid, F.S., 2020. Remediation of soil and water contaminated with petroleum hydrocarbon: a review. *Environ. Technol. Innov.* 17, 100526.
- Pakpahan, E.N., Isa, M.H., Kutty, S.R.M., Chantara, S., Wiriy, W., 2013. Polycyclic aromatic hydrocarbon removal from petroleum sludge cake using thermal treatment with additives. *Environ. Tech.* 34, 407–416.
- Ren, J., Song, X., Ding, D., 2020. Sustainable remediation of diesel-contaminated soil by low temperature thermal treatment: Improved energy efficiency and soil reusability. *Chemosphere* 241, 124952.
- Salimi, M., Ghorbani, A., 2020. Mechanical and compressibility characteristics of a soft clay stabilized by slag-based mixtures and geopolymers. *Appl. Clay Sci.* 184, 105390.
- Shalabi, F.I., Asi, I.M., Qasrawi, H.Y., 2017. Effect of by-product steel slag on the engineering properties of clay soils. *J. King Saud Univ.-Eng. Sci.* 29, 394–399.
- Shinbara, T., Makino, T., Matsumoto, K., Mizuguchi, J., 2005. Complete decomposition of polymers by means of thermally generated holes at high temperatures in titanium dioxide and its decomposition mechanism. *J. Appl. Phys.* 98, 044909.
- Shinde, S.S., Bhosale, C.H., Rajpure, K.Y., 2013. Kinetic analysis of heterogeneous photocatalysis: role of hydroxyl radicals. *Catal. Rev.* 55, 79–133.
- Silva, M.J., Soares, S.A.R., Santos, I.D.F., Pepe, I.M., Teixeira, L.R., Pereira, L.G., et al., 2020. Optimization of the photocatalytic degradation process of aromatic organic compounds applied to mangrove sediment. *Heliyon* 6, e05163.
- Sliem, M.A., Salim, A.Y., Mohamed, G.G., 2019. Photocatalytic degradation of anthracene in aqueous dispersion of metal oxides nanoparticles: effect of different parameters. *J. Photochem. Photobiol. A: Chem.* 371, 327–335.
- Smarzewska, S., Guziejewski, D., 2021. Soil remediation technologies. In: Rahman, R.O.A., Hussain, C.M. (Eds.), *Handbook of Advanced Approaches Towards Pollution Prevention and Control*. Elsevier, Amsterdam, pp. 193–219.
- Su, G., Li, Q., Lu, H., Zhang, L., Huang, L., Yan, L., et al., 2015. Thermal catalytic oxidation of octachloronaphthalene over anatase TiO₂ nanomaterial and its hypothesized mechanism. *Sci. Rep.* 5, 17800.
- Sun, D., Chi, D., Yang, Z., Xing, Z., Chen, P., Li, Z., et al., 2020. CdS quantum dots modified surface oxygen vacancy defect ZnO_{1-x}-TiO_{2-x} solid solution sphere as Z-Scheme heterojunctions for efficient visible light-driven photothermal-photocatalytic performance. *J. Alloy. Compd.* 826, 154218.
- Tao, Q., Bi, J., Huang, X., Wei, R., Wang, T., Zhou, Y., et al., 2021. Fabrication, application, optimization and working mechanism of Fe₂O₃ and its composites for contaminants elimination from wastewater. *Chemosphere* 263, 127889.
- Teng, D., Mao, K., Ali, W., Xu, G., Huang, G., Niazi, N.K., et al., 2020. Describing the toxicity and sources and the remediation technologies for mercury-contaminated soil. *RSC Adv.* 10, 23221–23232.
- Thuan, N.T., Chang, M.B., 2012. Investigation of the degradation of pentachlorophenol in sandy soil via low-temperature pyrolysis. *J. Hazard. Mater.* 229–230, 411–418.
- Tournassat, C., Bizi, M., Braibant, G., Crouzet, C., 2011. Influence of montmorillonite tactoid size on Na-Ca cation exchange reactions. *J. Coll. Interface Sci.* 364, 443–454.
- Tsai, T.T., Kao, C.M., 2009. Treatment of petroleum-hydrocarbon contaminated soils using hydrogen peroxide oxidation catalyzed by waste basic oxygen furnace slag. *J. Hazard. Mater.* 170, 466–472.
- Ueta, I., Mizuguchi, A., Tani, K., Kawakubo, S., Saito, Y., 2014. Evaluation of thermal catalytic decomposition of organic compounds with TiO₂ by packed-capillary gas chromatography. *Analyst. Sci.* 30, 407–412.
- US EPA (United States Environmental Protection Agency), 2019. Environmental contaminants often found at brownfield sites. <https://nepis.epa.gov/Exe/ZyPURL.cgi?Dockey=P100XPDD.txt>.
- Ureña, C., Azañón, J.M., Corpas, F., Nieto, F., León, C., Pérez, L., 2013. Magnesium hydroxide, seawater and olive mill wastewater to reduce swelling potential and plasticity of bentonite soil. *Constr. Build. Mater.* 45, 289–297.
- Usman, M., Faure, P., Hanna, K., Abdelmoula, M., Ruby, C., 2012. Application of magnetite catalyzed chemical oxidation (Fenton-like and persulfate) for the remediation of oil hydrocarbon contamination. *Fuel* 96, 270–276.
- Valizadeh, S., Lee, S.S., Baek, K., Choi, Y.J., Jeon, B.H., Rhee, G.H., et al., 2021. Bioremediation strategies with biochar for polychlorinated biphenyls (PCBs)-contaminated soils: a review. *Environ. Res.* 200, 111757.
- Valizadeh, S., Lee, S.S., Choi, Y.J., Baek, K., Jeon, B.H., Andrew Lin, K.Y., et al., 2022. Biochar application strategies for polycyclic aromatic hydrocarbons removal from soils. *Environ. Res.* 213, 113599.
- Vidonish, J.E., Zygourakis, K., Masiello, C.A., Sabadell, G., Alvarez, P.J.J., 2016. Thermal treatment of hydrocarbon-impacted soils: A review of technology innovation for sustainable remediation. *Engineering* 2, 426–437.
- Vitale, E., Deneele, D., Russo, G., 2020. Microstructural investigations on plasticity of lime-treated soils. *Minerals* 10, 386.
- Wan, X., Yang, J., Huang, X., Tie, S., Lan, S., 2019. A high-performance room temperature thermocatalyst Cu₂O/Ag⁰@Ag-NPs for dye degradation under dark condition. *J. Alloy. Compd.* 785, 398–409.
- Wang, A., Teng, Y., Hu, X., Wu, L., Huang, Y., Luo, Y., et al., 2016. Diphenylarsinic acid contaminated soil remediation by titanium dioxide (P25) photocatalysis: Degradation pathway, optimization of operating parameters and effects of soil properties. *Sci. Total Environ.* 541, 348–355.
- Wang, B., Wu, A., Li, X., Ji, L., Sun, C., Shen, Z., et al., 2021. Progress in fundamental research on thermal desorption remediation of organic compound-contaminated soil. *Waste Disposal Sustain. Energy* 3, 83–95.
- Wang, C., Astruc, D., 2014. Nanogold plasmonic photocatalysis for organic synthesis and clean energy conversion. *Chem. Soc. Rev.* 43, 7188–7216.
- Wang, R., Yuan, Y., Yen, H., Grieneisen, M., Arnold, J., Wang, D., et al., 2019a. A review of pesticide fate and transport simulation at watershed level using SWAT: current status and research concerns. *Sci. Total Environ.* 669, 512–526.
- Wang, J., Luo, Z., Song, Y., Zheng, X., Qu, L., Qian, J., et al., 2019b. Remediation of phenanthrene contaminated soil by g-C₃N₄/Fe₃O₄ composites and its phytotoxicity evaluation. *Chemosphere* 221, 554–562.

- Wang, Y., Liu, C.S., Li, F.B., Liu, C.P., Liang, J.B., 2009. Photodegradation of polycyclic aromatic hydrocarbon pyrene by iron oxide in solid phase. *J. Hazard. Mater.* 162, 716–723.
- Wang, Z., Jia, H., Zheng, T., Dai, Y., Zhang, C., Guo, X., et al., 2020. Promoted catalytic transformation of polycyclic aromatic hydrocarbons by MnO₂ polymorphs: synergistic effects of Mn³⁺ and oxygen vacancies. *Appl. Catal. B: Environ.* 272, 119030.
- Wey, M.Y., Liu, K.Y., Yu, W.J., Lin, C.L., Chang, F.Y., 2008. Influences of chlorine content on emission of HCl and organic compounds in waste incineration using fluidized beds. *Waste Manag.* 28, 406–415.
- Widmann, D., Behm, R.J., 2018. Dynamic surface composition in a Mars-van Krevelen type reaction: CO oxidation on Au/TiO₂. *J. Catal.* 357, 263–273.
- Xiao, Z., Guo, S., Cheng, F., Wang, S., 2022. Effects of mineral species and petroleum components on thermal desorption behavior of petroleum-contaminated soil. *Chemosphere* 307, 135548.
- Xu, X., Ji, F., Fan, Z., He, L., 2011. Degradation of glyphosate in soil photocatalyzed by Fe₃O₄/SiO₂/TiO₂ under solar light. *Int. J. Environ. Res. Public Health* 8, 1258–1270.
- Yang, Q., Tan, G., Zhang, B., Feng, S., Bi, Y., Wang, Z., et al., 2023. Cs_{0.33}WO₃/(t-m)-BiVO₄ double Z-type heterojunction photothermal synergistic enhanced full-spectrum degradation of antibiotics. *Chem. Eng. J.* 458, 141378.
- Yu, K., Sheng, G.D., McCall, W., 2016. Cosolvent effects on dechlorination of soil-sorbed polychlorinated biphenyls using bentonite clay-templated nanoscale zero valent iron. *Environ. Sci. Technol.* 50, 12949–12956.
- Yu, S., Du, B., Baheiduola, A., Geng, C., Liu, J., 2020. HCB dechlorination combined with heavy metals immobilization in MSWI fly ash by using n-Al/CaO dispersion mixture. *J. Hazard. Mater.* 392, 122510.
- Zhai, L.F., Duan, M.F., Qiao, M., Sun, M., Wang, S., 2019. Electro-assisted catalytic wet air oxidation of organic pollutants on a MnO@C/GF anode under room condition. *Appl. Catal. B: Environ.* 256, 117822.
- Zhang, J., Zhang, Y., Wang, R., Chen, H., Zhang, M., Zhang, J., 2018. Predication of the sources of particulate polycyclic aromatic hydrocarbons in China with distinctive characteristics based on multivariate analysis. *J. Clean. Prod.* 185, 841–851.
- Zhang, L., Li, P., Gong, Z., Li, X., 2008. Photocatalytic degradation of polycyclic aromatic hydrocarbons on soil surfaces using TiO₂ under UV light. *J. Hazard. Mater.* 158, 478–484.
- Zhang, L.H., Li, P.J., Gong, Z.Q., Oni, A.A., 2006. Photochemical behavior of benzo[a]pyrene on soil surfaces under UV light irradiation. *J. Environ. Sci.* 18, 1226–1232.
- Zhang, Y., Zhang, N., Wang, T., Huang, H., Chen, Y., Li, Z., et al., 2019. Heterogeneous degradation of organic contaminants in the photo-Fenton reaction employing pure cubic β -Fe₂O₃. *Appl. Catal. B: Environ.* 245, 410–419.
- Zhang, Z., Chen, K., Liu, D., Lou, B., Li, M., Guo, S., et al., 2021a. Comparative study of the carbonization process and structural evolution during needle coke preparation from petroleum and coal feedstock. *J. Anal. Appl. Pyrolysis* 156, 105097.
- Zhang, M., Cai, S., Li, J., Elimian, E.A., Chen, J., Jia, H., 2021b. Ternary multifunctional catalysts of polymeric carbon nitride coupled with Pt-embedded transition metal oxide to enhance light-driven photothermal catalytic degradation of VOCs. *J. Hazard. Mater.* 412, 125266.
- Zhao, C., Dong, Y., Feng, Y., Li, Y., Dong, Y., 2019a. Thermal desorption for remediation of contaminated soil: a review. *Chemosphere* 221, 841–855.
- Zhao, T., Xing, Z., Xiu, Z., Li, Z., Chen, P., Zhu, Q., et al., 2019b. Synergistic effect of surface plasmon resonance, Ti³⁺ and oxygen vacancy defects on Ag/MoS₂/TiO_{2-x} ternary heterojunctions with enhancing photothermal catalysis for low-temperature wastewater degradation. *J. Hazard. Mater.* 364, 117–124.
- Zhao, Z., Ni, M., Li, X., Buekens, A., Yan, J., 2017. PCDD/F formation during thermal desorption of p,p'-DDT contaminated soil. *Environ. Sci. Pollut. Res.* 24, 13659–13665.
- Zhu, D., Cai, L., Sun, Z., Zhang, A., Héroux, P., Kim, H., et al., 2021. Efficient degradation of tetracycline by RGO@black titanium dioxide nanofluid via enhanced catalysis and photothermal conversion. *Sci. Total Environ.* 787, 147536.
- Zhu, Z., Zhong, L., Zhang, Z., Li, H., Shi, W., Cui, F., et al., 2017. Gravity driven ultrafast removal of organic contaminants across catalytic superwetting membranes. *J. Mater. Chem. A* 5, 25266–25275.